Published in final edited form as:
Traffic. 2014 December ; 15(12): 1344–1365. doi:10.1111/tra.12229.

Copper Directs ATP7B to the Apical Domain of Hepatic Cells via Basolateral Endosomes

Lydia K. Nyasae, **Michael J. Schell**, and **Ann L. Hubbard**[1]

Ann L. Hubbard: alh@jhmi.edu

[1]Department of Cell Biology, The Johns Hopkins School of Medicine. 725 N. Wolfe St, Baltimore, MD 20184

Abstract

Physiologic Cu levels regulate the intracellular location of the Cu ATPase ATP7B. Here, we determined the routes of Cu-directed trafficking of endogenous ATP7B in the polarized hepatic cell line WIF-B and in the liver *in vivo*. Copper (10 μM) caused ATP7B to exit the trans-Golgi network (TGN) in vesicles, which trafficked via large basolateral endosomes to the apical domain within one hour. Although perturbants of luminal acidification had little effect on the TGN localization of ATP7B in low Cu, they blocked delivery to the apical membrane in elevated Cu. If the vesicular proton-pump inhibitor bafilomycin-A1 (Baf) was present with Cu, ATP7B still exited the TGN, but accumulated in large endosomes located near the coverslip, in the basolateral region. Baf washout restored ATP7B trafficking to the apical domain. If ATP7B was staged apically in high Cu, Baf addition promoted the accumulation of ATP7B in subapical endosomes, indicating a blockade of apical recycling, with concomitant loss of ATP7B at the apical membrane. The retrograde pathway to the TGN, induced by Cu removal, was far less affected by Baf than the anterograde (Cu-stimulated) case. Overall, loss of acidification impaired Cu-regulated trafficking of ATP7B at two main sites: 1) sorting and exit from large basolateral endosomes and 2) recycling via endosomes near the apical membrane.

Keywords

Wilson's Disease; hepatocytes; endosomes; proton ATPase; bafliomycin-A1; polarity; bile canaliculus; retromer

Introduction

Copper (Cu) is essential for life because it is a cofactor for certain oxidative enzymes, including superoxide dismutase, cytochrome oxidase, tyrosinase, lysyl oxidase, and ceruloplasmin. However, excess Cu in cells is toxic (1). Thus, cellular Cu homeostasis is highly regulated and is achieved in part by two intracellular Cu-transporting P-Type ATPases, ATP7A and ATP7B (2). When Cu is low, these proteins pump cytosolic Cu into the luminal spaces in the secretory pathway to supply Cu to newly synthesized

Correspondence to: Ann L. Hubbard, alh@jhmi.edu.

cuproenzymes. When Cu levels rise, Cu ATPases exit the trans-Golgi network (TGN) in vesicles and move near the plasma membrane, where they extrude Cu from the cell.

Menkes and Wilson's Diseases result from loss-of-function mutations in ATP7A and ATP7B, respectively (3). In Wilson's Disease, loss of ATP7B function leads to excess Cu accumulation in the brain, kidney and particularly the liver, due to defective biliary Cu excretion across the apical surface of hepatocytes. ATP7B in hepatocytes shows Cu-regulated localization *in vivo* (4). The trafficking mechanisms that operate physiologically during Cu-directed trafficking of ATP7B in hepatocytes remain poorly understood. We recently identified a Wilson's Disease mutation that affects the intracellular trafficking of ATP7B, while having little effect on ATPase activity itself, indicating that a mis-localization of ATP7B is sufficient to cause Wilson's Disease (5).

The physiologic maintenance of luminal pH is critical for intracellular trafficking (6). Luminal pH acidifies from ∼pH 6.0 in the Golgi to pH 5.5 in exocytotic vesicles nearing the cell surface. In the endocytic pathway, luminal pH forms a gradient beginning with pH ∼6.5 in early endosomes to between pH 6 and 5.5 in late endosomes and lysosomes. Organelle acidification is driven primarily by V-ATPase, a large multisubunit, ATP-dependent proton pump (7). Bafilomycin-A1 (Baf), a fungal metabolite, specifically inhibits V-ATPase activity at nanomolar concentrations (7, 8). Both Baf and weak bases perturb membrane trafficking, as they disperse pH gradients and in the process disrupt both intracellular location and receptor-ligand dissociation (9-12).

Previous studies, using a variety of overexpression systems and cell lines, have reached different and sometimes conflicting conclusions about the localization and trafficking itinerary of ATP7B (13-19). The present study focuses on endogenous ATP7B, in a cell model for polarized hepatocytes, which are the chief cells that express ATP7B *in vivo*. Our main finding is that in high Cu, endogenous ATP7B traverses endosomes near the basolateral domain en route to the apical plasma membrane. Furthermore, luminal acidification was required for the cell to redirect ATP7B to the apical domain via this pathway and maintain it there under conditions of high Cu.

Results

Cu levels regulate the reversible trafficking of endogenous ATP7B in polarized WIF-B cells

Free Cu levels in normal human blood are about 1 μM and are 10 to 50-fold higher in Wilson's Disease patients (20). In our initial study of ATP7B in WIF-B cells, we treated cells with 200 μM Cu for 4 hours and observed Cu-directed trafficking of both endogenous and exogenous ATP7B (19). However, exposing cultured cells to super-physiological levels of Cu for periods of hours is unlikely to model the *in vivo* situation with fidelity. In hepatocytes *in vivo*, endogenous ATP7B should respond to Cu concentrations typically seen in the blood, and the redistribution towards the apical domain should occur with sufficiently rapid kinetics to avoid Cu toxicity. Indeed, in primary cultures of hepatocytes, endogenous ATP7B redistributes to vesicles within 15 minutes of exposure to Cu (4). We thus sought conditions for ATP7B trafficking in WIF-B cells that were more analogous to the physiologic situation. In a previous study, we discovered that exposing WIF-B cells to 10

μM Cu was sufficient to redirect exogenous GFP-ATP7B to the apical region (13). We tested the suitability of this condition for studying the Cu-induced trafficking of endogenous ATP7B during the first hour of Cu exposure (Figure 1).

When cells were depleted of Cu following an overnight incubation in 10 μM of the cell-impermeable Cu chelator bathocuproine sulfonate (BCS), fixed, and stained with antibodies against ATP7B, the protein was predominantly in the TGN and overlapped with the post-TGN marker syntaxin 6 (Figure 1A-C). When WIF-B cells were transferred to 10 μM $CuCl_2$ for 60 minutes, most of the ATP7B was localized to the apical region marked by aminopeptidase N (APN) but also became more prominent in puncta dispersed in the cytoplasm (Figure 1D-F). When Cu-treated cells were subsequently incubated in 10 μM BCS for 3 hours, ATP7B returned to the TGN region (Figure 1G-I). Colocalization analysis (Figure 1J) confirmed that the fraction of cellular ATP7B that colocalized with the TGN marker decreased from 72% in BCS to 17% after 60 minutes in Cu, with a concomitant increase in overlap with the apical marker from 7% to 78%. Returning Cu-treated cells to the chelation condition completely restored the predominantly Golgi localization within 3 hours. Thus, WIF-B is a good model with which to study the physiological trafficking of endogenous ATP7B in hepatocytes, the chief cells expressing it *in vivo*.

Cu induces an increase in the number of ATP7B vesicles, which traverse large basolateral endosomes en route to the apical domain

In addition to the prominent localization of ATP7B in the Golgi when WIF-B cells were grown in BCS, they also exhibited a minor pool of ATP7B in puncta (Figure 2A'). These structures appeared much smaller than the TGN and they localized predominantly in confocal planes near the coverslip, i.e., the peripheral planes, which correspond to basal membrane attached to the substrate (Figure 2I). As shown in Figure 2C', when WIF-B cells were exposed to Cu for various times and then fixed and stained with antibodies to ATP7B, localization in the TGN diminished concomitant with an increased number of small ATP7B puncta, which arose prior to appearance of ATP7B in the apical region (Figure 2C'). We used 3D object analysis to estimate the number of small ATP7B vesicles per WIF-B cell (Figure 2G). Addition of Cu approximately triples the number of ATP7B vesicles/cell at 15 minutes—from 50 to 150. At longer times of exposure to Cu, when the majority of the ATP7B had reached the apical domain (Figure 2E), the number of circulating ATP7B vesicles diminished somewhat, yet the number remained double what it was during Cu chelation.

In preliminary experiments, we screened a range of antibodies that demark various intracellular compartments involved in the vesicular trafficking. No marker was found that showed an obviously high level of overlap with ATP7B in trafficking intermediates during its Cu-induced redistribution. However, a number of proteins involved in intracellular trafficking showed partial overlap, including: 1) Vti1b, a Qb-SNARE involved in vesicle fusion and, 2) the endosomal marker EEA1. We focused on EEA1 because it is a well-studied intracellular marker that selectively binds endosomal membranes rich in the lipid phosphatidyl inositol 3-phosphate (PI3P), the product of the conserved endosomal protein VPS34. In earlier studies, we demonstrated that the VPS34 lipid product is critical for the

function of distinct pools of endosomes located near the basolateral and apical membranes of WIF-B cells (21).

When WIF-B cells were incubated with Cu for various times then fixed and double- stained for ATP7B (green) and EEA1 (red) (Figure 2B, D & F), some intracellular membranes, especially in confocal planes located near the coverslip (Figure 2B', D' & F'), appeared positive for both markers, as indicated by yellow regions (Figure 2D'). Colocalization analysis (Figure 2H) showed that the fraction of ATP7B that overlapped with EEA1 more than doubled during the first 15 minutes of exposure to Cu. When all of the EEA1 structures in the cell were digitally binned into either “small vesicular” endosomes (cross-sectional area between 0.1 and 1 μm^2) or “large sorting” endosomes (area >1 μm^2), the majority of the total cellular EEA1 (60%) occurred in the “small vesicular” pool, with the remainder in larger structures. However, the flux of ATP7B induced by Cu appeared exclusively in the *larger* EEA1 compartments, with no increased colocalization in the vesicular pool of EEA1 at any time after Cu exposure. When incubated in Cu longer than 15 minutes, the fractional overlap of ATP7B with EEA1 gradually returned to its starting (Cu chelation) value of about 20% by 90 minutes in Cu (Figure 2H). Thus, following the addition of Cu, TGN-derived ATP7B traverses a large EEA1-positive endosomal compartment en route to the apical domain.

Because the confocal images indicated that the preponderance of TGN-derived ATP7B vesicles were located in planes near the coverslip in WIF-B cells (i.e., the peripheral planes, which correspond to basal membrane attached to the substrate, Figure 2C'), we devised an analysis method to plot the normalized location of cellular markers in the axial plane (Figure 2I-K). The total fluorescence intensity attributed to each marker was normalized across all slices in the stack (i.e., the whole cell), which allowed us to plot the peak expression of each marker in z-orientation (Figure 2J). The Golgi region, demarked by TGN38, showed peak fluorescence at approximately 5 μm from the coverslip, while the apical marker APN showed a broader peak, with a maximal fluorescence at about 6 μm above the coverslip. In contrast, endosomes demarked by EEA1 peaked at 2 μm—about 6 confocal planes closer to the coverslip compared to the Golgi and apical markers.

Axial distribution analysis of the cellular pool of ATP7B under Cu-chelation conditions produced a profile very similar to TGN38 (Figure 2K, green). In contrast, after 15 minutes in Cu, the distribution of ATP7B had shifted much closer to the coverslip/basolateral pole of the cell and became very similar to EEA1 (Figure 2K, red). By 90 minutes in Cu, the ATP7B distribution had assumed a profile similar to the apical marker APN (Figure 2K, blue). Thus, the large endosomal compartments traversed by ATP7B following Cu are concentrated near the coverslip in WIF-B cells, which corresponds to the blood sinusoidal/ basolateral domain of hepatocytes *in vivo* (22).

We wondered if a similar trafficking itinerary (Golgi to basolateral endosome to apical domain) occurred in hepatocytes *in vivo* after Cu. To test this, rats raised on a Cu-deficient diet were given Cu then sacrificed after 0, 1, or 2 hours. Figure 3 shows liver cryosections triple-immunostained for ATP7B (Figure 3 A,D,G, green), TGN38 (Golgi, B, E, H, red) or DPP4 (apical, B, E H, blue). In Figure 3J, we quantified the concomitant decrease in Golgi

localization and increase in apical localization that occurs after Cu. By 2 hours after Cu treatment, the majority of ATP7B colocalized with the apical marker DPP4. The arrows (Figure 3 D-F) indicate the transient appearance of ATP7B near the basolateral domain following 1-hr of Cu-administration *in vivo*.

The transient basolateral pool of ATP7B in hepatocytes was more easily observed in 3D renderings. Movie S1 depicts rendered confocal stacks at 0, 1, and 2 hours after Cu. ATP7B fluorescence is in green, with the areas of ATP7B that overlap with the apical marker DPP4 highlighted in cyan. Consistent with the colocalization analysis (Figure 3J), we observed a small pool (about 18% of the cellular total) of ATP7B that appeared coincident with the apical marker even in the low Cu condition *in vivo*. The line of red arrows in the 1 hour 3D image demarks a population of non-Golgi non-apical ATP7B, which appears transiently in the basolateral region at 1 hour after Cu and is the pool presumably en route to the apical domain. By 2 hours, this pool is diminished (3D image on right). Thus, the unique Cu-directed trafficking pathways of ATP7B appear similar in polarized WIF-B cells and in hepatocytes *in vivo*.

De-acidification prevents Cu-directed delivery to apical domain

Intracellular trafficking and sorting via endosomes requires precise physiological control of luminal pH, which depends critically on proton pumping by V-ATPases. Disruption of luminal pH gradients perturbs intracellular trafficking in a range of cells and tissues (23). We tested whether disruption of luminal pH affected the intracellular trafficking of ATP7B. Figure S2 depicts WIF-B cells treated with three different perturbants known to neutralize luminal pH. Cells were labeled by uptake of the cellular dye DAMP [3 (2,4-dinitroanilino)-3′-amino-N-methyldipropylamine], which accumulates physiologically in acidic intracellular compartments (panel A). Cells treated with Baf, chloroquine (CQ) or NH_4Cl (panels B-D) showed almost complete loss of acidic compartments.

Figure 4 illustrates how de-acidification affects Cu-directed apical delivery of ATP7B. When the pH pertubants were present for 30 minutes under Cu-chelation conditions, the fraction of ATP7B coincident with TGN38 did not change appreciably (Figure 4M, left set of bars). In contrast, when the perturbants were present during the 1-hour Cu exposure, each prevented Cu-directed apical delivery (Figure 4M, right set of bars). In all cases, apical delivery was reduced to below 20% of control levels, with Baf being the most efficacious (93% reduction in apical delivery). Thus maneuvers that disrupt luminal pH via different mechanisms show the common property of blocking apical delivery, suggesting that it is low pH itself—rather than a selective, pH-independent effect of Baf on the V-ATPase (24)—that is responsible for the blockade of ATP7B's Cu-directed apical delivery.

To further explore the apparent lack of effects of Baf when Cu is chelated, we treated WIF-B cells with BCS + 50 nM Baf for 4 hours, and refreshed Baf once per hour in case the drug was rapidly metabolized by the cells (Figure S3). If cells were kept in chelator, de-acidification, even for 4 hours, had only a modest effect on ATP7B localization. The degree of overlap with the post-Golgi marker syntaxin 6 was modestly reduced from 47% to 35%, but the number of circulating ATP7B vesicles was not affected by a 4-hour treatment in BCS + Baf. Thus, the effect of luminal acidification on ATP7B trafficking was remarkably

selective for the Cu-directed pathway, suggesting that the sorting mechanisms that redirect ATP7B to the apical domain when Cu levels rise require luminal pH gradients, while retention and/or recycling of ATP7B at the TGN in low Cu do not.

Baf causes ATP7B to accumulate in large endosomes at the basal end of the cell

Figure 4L' depicts single-plane images of large, heterogeneous ATP7B-positive compartments that form predominantly in confocal sections near the coverslip in WIF-B cells after a 1-hour Cu-treatment in the presence of Baf. Analysis of the axial distribution of ATP7B in these cells confirmed that Cu-directed ATP7B accumulates near the coverslip, preventing delivery to the apical membrane (Figure 4N, gray line). In Figure 5, we characterized the large basal EEA1 structures in more detail. Panels 5A-C depict a typical group of five ATP7B clusters co-labeled for EEA1 (each cluster approximately 5 μm in diameter). The clusters were already apparent as early as 15 minutes after Cu + Baf exposure. By 60 minutes in the presence of Baf and Cu, ATP7B had accumulated in 2 distinct pools of EEA1-positive large endosomes, apical and basolateral (Figure 5E and E').

To characterize the Baf-induced ATP7B clusters, we created masks to isolate the large EEA1-positive structures, which formed quickly upon exposure to Baf and were more homogeneously labeled across the cluster when labeled by antibodies to EEA1 compared to ATP7B (compare Figure 5A versus 5B). Focusing on EEA1 large structures allowed for a more robust particle analysis. Following exposure to Baf, nearly 100% of these large clusters were triple-positive for ATP7B, EEA1, and Vti1b. When we size-segregated small and large EEA1 compartments as done previously in our analysis of Cu-directed intermediates, a remarkable fraction (∼70%) of the ATP7B in the cell was localized to the large compartments by 60 minutes in Cu + Baf (Figure 5F). Conversely, the amount of ATP7B localized to the EEA1 small (vesicular) compartment decreased to <5% (Figure 5F, dotted line), compared to ∼10% in controls (Figure 2H, dotted line).

Baf treatment also affected the size of large EEA1 structures themselves (Figure 5G). The mean cross-sectional area of the large structures (those with an area greater than 1 μm^2) approximately doubled, from 2 to 4 μm^2, while the fraction of the total EEA1 pool that accounted for them also doubled, from about 40% to 80% (Figure 5H). Baf also caused an obvious reduction in the abundance of small, vesicular-like EEA1 structures; this was not quantified. The overall effect of Baf on EEA1 was to promote a pooling and accumulation of the protein into large endosomal compartments.

Within the large clusters shown in Figure 5 A-C, it was clear that ATP7B and EEA1 were distributed heterogeneously, suggesting micro-organization of the membrane. Specifically, it was unclear if the ATP7B punctae occurred in continuity with the main EEA1 compartment or rather consisted of closely associated, but distinct vesicles. It was also unclear whether the EEA1 was organized as one big structure or consisted of aggregates of smaller vesicles. To address these questions, we applied a confocal/deconvolution technique that used a higher pixel density and a smaller pinhole to increase our ability to image these structures. We examined 3 time points (15, 30, and 60 minutes) after Cu+Baf treatment. Altogether, we analyzed 22 examples. Figure 6 shows an example of one of these structures. The overall dimensions among the structures showed considerable heterogeneity, especially at the 60

minute time point when the cross sectional area ranged between 3 and 28 μm^2 and their thicknesses varied between 1.5 and 3 μm. EEA1 and ATP7B typically exhibited a complementary relationship within the structures, and we sometimes observed what appeared to be distinct ATP7B vesicles (which were negative for EEA1) in the local vicinity of the main EEA1 structure, which appeared as a more contiguous tubular network. In Figure 6C, we show that the size of the structures increased over time in Cu+ Baf, confirming the prior analysis. Colocalization analysis (Figure 6D) indicated that the amount of ATP7B fluorescence that was coincident with EEA1 varied between 42 and 49% and did not change significantly with time of exposure to Cu + Baf. These data are consistent with a model in which Baf creates a blockade in the budding, pinching off, or tubulation processes that operate in high Cu to sort ATP7B from large, tubular EEA1+ endosomes, prior to delivery to the apical membrane.

Movie S4 provides a visual summary of the effects of Cu in the absence and presence of Baf. The top row of renderings shows ATP7B fluorescence merged with the red mask for the EEA1 large compartment. When Cu was added in the absence of Baf, a transient increase in overlap with EEA1 large (middle panel) was seen prior to apical delivery (right panel). The bottom row shows the accumulation of ATP7B in these large compartments as early as 15 minutes after Cu + Baf treatment, and more ATP7B accumulated there after 60 minutes. By manually counting these structures in 3D renderings, we estimated that the number of large Baf-induced EEA1 structures per cell is small—fewer than 10 per cell.

Baf washout restores Cu-directed apical localization

Since de-acidification inhibits degradative processes in lysosomes and can both inhibit (25) or enhance (26) autophagy, we wondered if the large EEA1 structures were created by changes in trafficking to these compartments. In Figure S5, we labeled the Baf-treated cells with markers against lysosomes (LAMP1, A-B), Cathepsin D (C-D) or autophagosomes (LC3B, E-F) and observed no overlap between these organelles and the ATP7B clusters. This result indicates that it is unlikely that ATP7B had accumulated in a degradative compartment.

Furthermore, if ATP7B had accumulated in terminal degradative compartments, then removal of the drug would not be expected to restore apical delivery. Figure 7 shows that the blockade of ATP7B apical delivery produced by Baf is reversible following Baf washout. Baf exposure, even for 3 hours, did not affect ATP7B protein levels (Figure 7J). This indicates that changes in the rate of synthesis and degradation do not account for the effect of Baf on ATP7B trafficking. Moreover, the half-life of ATP7B in hepatic cells is ∼8 hours (27), which is considerably longer than the timeline of our experiments. Following washout, apically localized ATP7B became apparent by 3 hours (compare Figure 7C and E, with concurrent disappearance of the large ATP7B clusters in the periphery (7D' and F'). The effects of Baf washout were quantified in Figure 7G, H & I using the methods we developed to characterize Cu-directed trafficking. The accumulation in large structures near the coverslip was almost completely reversed (Figure 7I), and the number of circulating ATP7B vesicles was restored to control levels (Figure 7H). The restoration of apical delivery following Baf washout was also observed, but it was partial (Figure 7G). This is not

unexpected, owing to the high binding affinity of Baf for the V-ATPase, which has a dissociation constant (K_D) of $\sim 10^{-8}$ M (28). Overall, our results showed that, upon Baf washout in the presence of Cu, ATP7B could be rescued from the large peripheral structures and redirected towards the apical domain.

Baf blocks apical recycling, which maintains ATP7B at the apical surface

We next focused on the pathways involved in the maintenance of ATP7B at the apical membrane in Cu-treated cells (Figure 8). In these experiments, cells were treated for 1 hour with Cu to stage ATP7B at the apical domain, and then Baf was added in the continued presence of Cu. Baf caused a progressive loss of ATP7B colocalization with APN, in conjunction with increased colocalization with EEA1 (Figure 8H). The effect could be measured already after 30 minutes exposure to Baf (left panels), which suggests that significant amounts of apical ATP7B are recycling through subapical EEA1 endosomes in high Cu. The effect of Baf was more pronounced after 3 hours (right panels), when ∼70% of the apical colocalization was lost (Figure 8M), and ATP7B had accumulated in large endosomal structures throughout the cell. Quantitative Western blot of ATP7B (Figure 8N) showed no change in ATP7B protein levels during the assay, ruling out perturbed rates of degradation and/or new synthesis. Thus, our results suggest that ATP7B is actively maintained at the apical membrane via recycling, and that Baf causes a selective blockade in exocytosis from endosomes located near the apical plasma membrane.

Baf treatment does not inhibit Cu-dependent retrograde (apical to TGN) traffic of ATP7B

The effects of Baf on ATP7B localization appeared to be selective for ATP7B in the Cu-bound conformation. We wondered how Baf would affect ATP7B when Cu was removed, during the protein's return to the TGN. To do this, we staged cells in high Cu (as in Figure 8A) then added Baf or vehicle (as in Figure 8E or 8B, respectively), followed by Cu removal by incubating cells with Cu chelator for 3 hours. At various times after returning cells to low Cu condition, we fixed and stained cells for EEA1 or TGN38 to monitor retrograde traffic (apical to TGN; Figure 9). In control cells having normal luminal acidification, a majority of ATP7B returns to the TGN by 3 hours (Figure 9A-C). If Baf was present during the return (Figure 9D-F), the rate at which ATP7B repopulated the TGN was similar to control (Figure 9H). Although the presence of Baf approximately doubled the fraction of ATP7B that showed overlap with EEA1 at all times points (Figure 9G, compare solid and dotted lines), this change did not affect the rate of return to the Golgi in low Cu (Figure 9H). Thus, it appears that luminal acidification is a critical component of physiological ATP7B trafficking mainly when Cu is directing the protein to the apical domain and maintaining it there.

Discussion

A major finding of this study is that, in WIF-B cells, the Cu-directed trafficking of endogenous ATP7B occurs via large basolateral endosomes prior to appearance at the apical domain. The physiological relevance of this finding was validated in hepatocytes *in vivo*, where ATP7B exhibited a similar trafficking itinerary: TGN to the basolateral region to the bile canaliculus. A second major finding is that Cu-directed trafficking depends on luminal acidification at two main intracellular sites: exit from a basolateral sorting endosome and

exocytosis to the apical plasma membrane. In low Cu conditions, the localization of ATP7B was barely affected by loss of acidification. Yet, when Cu levels were raised, delivery to the apical domain was almost completely blocked. The exquisite sensitivity of ATP7B localization to luminal pH when Cu levels are high implies that pathological processes or mutations that disrupt luminal pH in hepatocytes would reduce the capacity for ATP7B-dependent Cu sequestration and extrusion into the bile, leading to Cu toxicity. Further study will be required to test this idea directly.

A summary of our findings in WIF-B cells is depicted in Figure 10. In low Cu, the majority of ATP7B (∼85%) is associated with the Golgi, with the remaining 15% in vesicles concentrated near the basolateral membrane—a localization that is analogous to the sinusoid, the site of Cu uptake from the blood in hepatocytes. If deacidification is induced under this condition, only minor effects on ATP7B localization occur. The ATP7B vesicles are positioned to function as Cu sentinels in the cytosol, near sites of Cu uptake from the blood and equipped with ATP7B for rapid Cu sequestration. In low Cu, we presume that these vesicles (∼50/ WIF-B cell) recycle to the TGN. In hepatocytes in low Cu, any Cu sequestered by such vesicles near the sinusoid would therefore be returned to the secretory pathway for use in metallation reactions.

When intracellular Cu levels rise, the number of ATP7B vesicles triples and the predominant Golgi-like localization of ATP7B disappears, as the protein is redirected apically; this would presumably increase the capacity for rapid Cu sequestration in the cytosol followed by extrusion at the apical membrane when Cu is in excess. Notably, even at long times of Cu exposure, the fractional overlap of ATP7B and TGN38 remained at 15%, which implies that ATP7B-dependent delivery of Cu to the TGN lumen persists in high Cu. Thus, when intracellular Cu levels are high, some ATP7B continues to return to the TGN but perhaps does not reside there long before exiting again as vesicles. A similar continual flux through the TGN in high Cu has been shown for ATP7A (29).

We find that endogenous ATP7B traverses large basal endosomes en route to the apical domain. A similar itinerary to the plasma membrane (via EEA1-positive endosomes) was suggested in another recent study, which used exogenous ATP7B in COS-7 cells (16). Once ATP7B exits the TGN, it appears to be committed to a trafficking route towards the basolateral domain prior to segregation and retrieval from large endosomes for apical delivery. The microtubules in polarized WIF-B cells are organized such that the plus ends localize near the basal membrane and the minus-end rich microtubule-organizing centers are located in close vicinity to the apical plasma membrane and Golgi (22). This strongly suggests that long-range transport of ATP7B is mediated by microtubule motors, both minus-end and plus-end directed, as suggested previously by a requirement for dynactin in ATP7B trafficking (30). We estimate that the distance an ATP7B molecule originating at the TGN must traverse to reach the apical membrane in a WIF-B cell is ∼7 μm; that is, 3 μm to go from TGN to basal endosomes, plus 3 μm to go from basal endosomes to apical region, plus 1 μm for apical delivery.

In Cu-treated cells exposed to different pH neutralizers, ATP7B vesicles still exited the TGN but they failed to reach the apical region. Instead, the protein accumulated in large

EEA1 endosomes, which themselves grew larger with increasing times in Baf. Within these structures, ATP7B and the endosomal marker EEA1 exhibited a complementary relationship and approximately 50% overlap (see Figure 6). Our experiments indicate that Cu-directed ATP7B trafficking involves a Baf-sensitive mechanism, which functions to segregate ATP7B out of large endosomes prior to retrieval and delivery to the apical region. The presence of Baf blocks one or more of the processes involved in segregation, budding, or tubulation from the main EEA1 structure, prior to the creation of cargo destined for the apical domain.

A number of previous studies of ATP7B have employed overexpressed protein (31) using non-polarized cells (32) and/or treated cells with Cu for as much as 10X longer and/or at a 10X higher concentration (18) than in the present study. Under conditions of pathological Cu overload, increased amounts of both Cu and lysosomal hydrolases appear in the bile, owing to Cu toxicity (33, 34). These studies have led to the suggestion that ATP7B resides physiologically in hepatic lysosomes, which fuse directly with the apical membrane. One recent report, which employed exogenous GFP-ATP7B in nonpolarized cells, concluded that secretory lysosomes are a major pathway for delivery of ATP7B to the plasma membrane (17). In our study, endogenous ATP7B in polarized WIF-B cells was not found in lysosomes. Our finding that ATP7B traverses sorting endosomes prior to retrieval to the apical domain suggests that the different results of previous studies are explained by saturation of the physiologic segregation and redirection systems in endosomes during super-physiological Cu conditions and/or if ATP7B is overexpressed. In such a scenario, ATP7B cargo would be expected to escape rescue from endosomes and accumulate non-physiologically in late endosomes or lysosomes.

In endosomes near the apical plasma membrane, we uncovered a second site of ATP7B sensitivity to Baf. Loss of luminal acidification blocked ATP7B recycling through apical endosomes. In the presence of Cu, Baf blocked exocytosis of ATP7B, preventing apical delivery. Thus physiologic luminal acidification is not only required for the apical targeting of ATP7B but also for its maintenance at the apical membrane in continued high Cu. A number of previous studies have shown a requirement for luminal acidification for exocytosis at the plasma membrane (35)

Based on the present results, one might hypothesize that *all* apical trafficking is blocked by deacidification. However the apical resident protein APN, which takes a transcytotic route (36) was not affected by Baf. In experiments where we compared ATP7B and APN (not shown), the amount of ATP7B found in the APN “small” compartment, which consists mainly of vesicles en route to the apical domain, was never more than 3%--nor did it change with Cu levels or following loss of luminal acidification. Additional experiments using continuous uptake of anti-APN from the basolateral surface of WIF-B cells showed that vesicles in the transcytotic pathway, which also target the apical surface (22), were successfully delivered in the presence of Baf and did not form large clusters as the apically targeted ATP7B did. Thus, the Cu-directed route of ATP7B is different from the route taken by newly synthesized resident apical proteins in hepatocytes.

What mediates the Baf-sensitive retrieval mechanism of ATP7B from large endosomes in high Cu? One attractive candidate mechanism involves retromer (37), which was recently shown to interact with ATP7A, the Menkes Disease protein (38). Retromer mediates minus-end directed cargo retrieval from EEA1-positive endosomes via the transient formation of tubules. We did not observe such tubules, but they are labile and may not be preserved in fixed cells. Our images of these structures are consistent with the idea that luminal acidification did not prevent the micro-segregation of ATP7B cargo within the endosomal membrane, but rather blocked the separation of this cargo prior to long-range trafficking to the apical domain. Interestingly, a genetic link between retromer-mediated trafficking and luminal pH has been shown in yeast (39, 40). Does the postendosomal itinerary of ATP7B proceed via vesicles, tubules, or both? In contrast to the apparently long distances traveled by ATP7B en route to the apical domain, the return trip (apical to Golgi) appears to be much shorter (<1 μm), owing to the close juxtaposition of the apical membrane and the Golgi. Live cell imaging, in conjunction with direct knockdown of retromer machinery, will be required to address these questions.

Materials and Methods

Materials

Bathocuproine disulfonic acid (BCS), cupric chloride ($CuCl_2$), Bafilomycin-A1 (Baf), chloroquine (CQ), dimethyl sulfoxide (DMSO), imidazole, AEBSF and Pipes were purchased from Sigma (St. Louis, MO) while ammonium chloride (NH_4Cl) was from J.T. Baker (Phillipsburg, NJ). NuPAGE Novex 4-12% gradient Bis-Tris gels and MOPS SDS Running buffer were from Invitrogen (Carlsbad, CA), while PVDF Immobilon-P membrane was from Millipore (Bedford, MA). Halt protease inhibitors and West Pico super signal substrate were from Thermo Scientific (Rockford, IL). All other chemicals were of the highest purity and obtained from sources identified in previous publications.

Antibodies

Primary antibodies used for indirect immunofluorescence were as follows: for Figures 1, 4, S5, and 6 we used rat anti-ATP7B (S. Lutsenko, Johns Hopkins School of Medicine); For Figures 2, S3, S4, 5, 7 & 8 we used rabbit anti-ATP7B (#ab124973, Abcam, Cambridge, MA); for Figures 3 and S1 we used rabbit anti-ATP7B (Dr. J. Gitlin, Brown Alpert Medical School, Providence, RI); rabbit anti-aminopeptidase N (APN, #1637, (22) guinea pig anti-dipeptidyl-peptidase 4 (DPP4, (41)) goat anti-EEA1 (#sc-6415, Santa Cruz Biotechnology, Santa Cruz, CA); mouse anti-TGN38, and -Syntaxin 6 (BD Biosciences, San Jose, CA); mouse anti-LAMP1 (#H4A3-s, Developmental Studies Hybridoma Bank, Iowa City, IA); rabbit anti-Cathepsin D (Dr A. Hasilik, Marburg, Germany); rabbit anti-LC3B (#2775, Cell Signaling Technology, Danvers, MA). Secondary antibodies conjugated to Cy3 or Cy5 were from Jackson ImmunoResearch Laboratories (West Grove, PA), while those conjugated to Alexa 488, -568 or -647 were from Molecular Probes (Eugene, OR). Primary antibodies used for immunoblotting inculded: rabbit anti-ATP7B (#3985) (13), mouse anti-alpha tubulin, DM1A (Sigma, St. Louis, MO). Secondary antibodies conjugated to horseradish peroxidase (HRP) were from G.E. Healthcare (Buckinghamshire, United Kingdom).

Cell Culture

WIF-B cells were seeded at 2×10^4 cells/cm^2 on glass coverslips (22 × 22 mm), cultured as described (22, 42) and used at 11–13 days later when maximal polarity had been achieved.

Anterograde and retrograde trafficking assays

For ATP7B anterograde trafficking, cells were incubated overnight in 10 μM BCS to stage ATP7B at the TGN then fixed, while a parallel set was rinsed and switched to 10 μM $CuCl_2$ for 60 minutes to direct ATP7B to the apical region, then fixed. In some cases, cells were fixed every 15 minutes during the 1-hour Cu treatment (Figure 2). For ATP7B retrograde (apical region-to-TGN) traffic, cells were treated as above, then rinsed and incubated in 10 μM BCS for 180 minutes to promote ATP7B return to the TGN.

Bafilomycin-A1 (Baf), chloroquine (CQ) and ammonium chloride (NH_4Cl) treatments

50 nM Baf, 300 μM CQ or 30 mM NH_4Cl were added to BCS- or Cu-media 30 minutes prior to and during anterograde or retrograde trafficking assays. Controls were treated with DMSO (up to 0.05% final concentration). For ATP7B retrograde traffic in the presence of Baf (Figure 9), cells exposed to 10 μM $CuCl_2$ for 60 minutes were treated an additional 30 minutes in Cu plus Baf or vehicle, then switched to BCS for 180 minutes, in the continued presence of Baf or vehicle. Prolonged treatment with Baf was used in some experiments to examine ATP7B steady state localization at the TGN (BCS-treated cells; Figure S3) or apical region (Cu-treated cells; Figure 8). For assays in chelator, cells were treated overnight in 10 μM BCS to stage ATP7B at the TGN and incubated an additional 240 minutes in BCS plus Baf then fixed. For assays in Cu, cells were treated in Cu for 60 minutes to stage ATP7B at the apical region and incubated up to an additional 180 minutes in Cu plus Baf, then fixed (Figure 8K). Parallel sets of cells, in duplicate, were used as samples in Western blots to assess ATP7B protein levels. In experiments where Baf was washed out to test reversibility, WIF-B cells were washed 3X with medium containing 10 μM $CuCl_2$ plus vehicle then incubated in Cu for an additional 3 hours. A parallel set of cells, in duplicate, were used as samples in Western blots to assess ATP7B protein levels

Copper-deficiency and copper-administration in vivo

Animal handling and experimental procedures were approved by the Johns Hopkins Animal Care and Use Committee. Copper-deficient Sprague-Dawley rat pups born to pregnant dams (Charles River Breeding Labs, Wilmington, MA) were fed a Cu-deficient chow (# TD. 80388, Harlan Tekland, Madison, WI) beginning at 5-7 days prenatal and during the weaning period. The weaned pups were maintained on the same chow until they were 38-45 days old. Before the exposure to Cu, the Cu-deficient rats were starved overnight, then Cu was administered via intraperitoneal injection of $CuSO_4$ in saline (3 mg Cu/Kg body weight). At 0, 1, 2, or 3 hr later, rats were lightly anesthetized, decapitated, and their livers excised. Livers were rinsed briefly in cold 0.9% saline, then cut into 5 × 20 mm blocks prior to immersion in fixative and cryosectioned as previously described (43). ATP7B was visualized with a rabbit polyclonal antibody (a gift of Dr. J. Gitlin).

Indirect immunofluorescence

For experiments that used the rat anti-ATP7B antibody, WIF-B cells were processed at room temperature as follows. Cells were briefly rinsed in PBS, fixed 30 minutes in 4% paraformaldehyde/PBS then permeabilized for 5 minutes in 0.2%Triton-X 100 in PHEM buffer (60 mM Pipes, 25 mM Hepes, 10 mM EGTA, and 2 mM $MgCl_2$, pH 6.8). Fixed and permeabilized cells were incubated for 30 minutes in blocking buffer (PBS containing 1% BSA and 0.1% Triton-X100), and incubated in primary antibodies (1 hour) and secondary antibodies (30 minutes) diluted in blocking buffer. For experiments that employed the rabbit polyconal ATP7B (#ab124973, Abcam) cells were fixed on ice and permeabilized as previously described (22).

Confocal Microscopy

Images were collected on a confocal microscope (Zeiss LSM 510 Meta), using a 100X oil objective (N.A.=1.4) and a pinhole size of one airy unit. We collected twelve-bit confocal image stacks (512 × 512 lateral dimensions; 0.176 × 0.176 μm pixels) of 18-25 slices at 0.4 μm Z-step sizes from dual- or triple labeled cells. Single plane images in the figures were collated with Adobe Photoshop and Illustrator CS5 software.

2D image analysis

Single channels from the confocal stacks were opened in Fiji, and the middle slice in the stack was auto-thresholded using the Triangle method (44); this threshold was applied to all images in the stack. Image J Particle counting was used to identify and classify particles in each slice with a cross-sectional diameter of 0.1 μm^2 or larger and create a binarized mask. Thus, the size cutoff considers structures in the slice 2 × 2 pixels or larger (0.124 μm^2), while particles with a cross-sectional area smaller than 0.1 μm^2 were assumed to be a mixture of sub-resolution cellular structures and noise and were not analyzed. In analyses where we segregated organelle size, particles having a cross-sectional area between 0.1 and 1 μm^2 were designated “small” and those with an area over 1 μm^2 area were “large.” The total fluorescence value for a given marker was calculated to be the sum of pixel intensity values in that channel's masked region. For colocalization analysis, pixels common to two masks were found by combining the masks for each channel using the Fiji image calculator “AND” function. Percent colocalization was expressed as the ratio of summed pixel values present in common mask divided by the summed pixel values in the ATP7B channel. Analyses were performed on between 3-12 confocal stacks obtained from between 1-5 independent experiments. In cases where analysis from a single experiment is shown, qualitatively similar results were observed in at least two independent replications.

Deconvolution confocal microscopy and analysis

WIF-B cells treated with 10 μm Cu + 50 nM Baf for 15, 30, and 60 minutes were fixed and labeled for ATP7B (green), EEA1 (red) and APN (blue). We used a Zeiss LSM 710 confocal microscope with the pinhole set to 0.5 airy units (green channel) to collect stacks in 0.25 μm Z-steps. Using a 5X digital zoom to focus on the large EEA1/ATP7B-positve structures located approximately 1-3 μm above the coverslip, we collected 16-bit images of dimensions 1024 × 1024 pixels, using a 100X N.A 1.4 oil objective. Thus, in this analysis,

the lateral dimensions of the pixels were 0.021 × 0.021 μm, which is nearly 10X smaller than what was used in the prior analyses. All stacks were collected from fully polarized WIF-B cells, as judged by the presence of an apical surface labeled by APN. The stacks were further subjected to 10 rounds of blind, reiterative 3D deconvolution using the default settings (medium noise) of the Autodeblur algorithm in the Autoquant package (version X, 1.4.1). Deconvolved images were exported as single-channel.tif images and imported into Fiji, where contrast was adjusted by use of a stack histogram, in which 0.1% of the pixels were saturated. To obtain dimensions of the structures and perform colocalzation analysis, individual structures were cropped from the original images and also cropped in the axial plane such that only structures located near the coverslip remained in the stack, while more nuclear planes were excluded. Dimensions of the structures in XY were measured from maximal projections of the EEA1 channel. Dimensions in Z were estimated by multiplying the number of Z-sections encompassing the structure by the step size (0.25 μm). Colocalization analysis for ATP7B and EEA1 was performed similarly to the other analyses, except that we did not size select the masks and the Otsu thresholding routine from Fiji was used. Images in Figure 6A are maximal Z-projections. Images In Figure 6B are single confocal planes. Altogether, we analyzed a total of 22 distinct EEA1/ATP7B structures over the 3 time points.

3D analysis

To estimate the number of ATP7B vesicles/cell, the binarized masks used in the 2D analysis were opened in Fiji and processed using in the 3D Particle Analyzer from the BoneJ plugin (45). Trial and error testing established that an object volume cutoff of 3 μm^3, which corresponds structures containing between 4-164 voxels (.176 × .176 × 0.4 μm dimensions), reliably segregated the TGN pool from the vesicular pool of ATP7B. Thus, objects called “vesicles” in this analysis had an estimated volume between .004 and 3 μm^3. Images were rendered in 3D using the 3D viewer in Fiji.

To estimate the number of cells in a microscopic field, the ATP7B fluorescence channel was used to identify and count the (unstained) nuclear profiles, including those from cells on the edges of the stack. The number of cells in the stack was estimated to be the number of full-cell nuclei in the stack plus half the number of those nuclei of cells at the edge of the stack. Among the stacks collected over multiple experiments, the estimated number of WIF-B cells per stack ranged from 19 to 33, with a mean of 27.5 +/- 6.2 (SD); N= 32 confocal stacks.

Digital analysis of distribution in the axial plane

To determine the z-distribution of a fluorescent label, the distribution of fluorescence units for each fluorescence channel after thresholding and masking (describe above) was expressed as the percent of total per slice in the stack. The closest slice to the coverslip showing detectable fluorescence was defined as being 0.4 μm above the coverslip (i.e., slice 1), and subsequent slices were spaced at 0.4 μm steps above. Thus, in these analyses the area under each curve equals 1 (the total fluorescence of that marker) defined by the summed pixel intensities contained within the mask.

Detection of acidic organelles using DAMP stain

The extent of deacidification by 50 nM Baf, 300 μM CQ or 30 mM NH_4Cl was confirmed using 3-(2,4-dinitroanilino)-3′-amino-N-methyldipropylamine (DAMP) labeling as described in (46), with some modifications. Briefly, WIF-B cells were incubated in basal media containing Baf, CQ or NH_4Cl for 30 minutes. DAMP (30 μM) was added for an additional 60 minutes in the continued presence of the drug in basal media. Cells were fixed for 30 min in 4% paraformaldehyde in PBS, permeabilized at room temperature for 5 minutes in 0.2% Tx100 in PHEM buffer, then blocked in 1% BSA/PBS for 30 minutes. Incubations with primary (Goat anti-DNP, Oxford Biomed Research) and secondary (Donkey anti-goat Cy3) antibodies were done at 37°C for 1 hour each in 1% BSA/PBS. Confocal images were acquired at the same laser, detector and pinhole settings to allow direct comparison of the fluorescent signal after each treatment.

Immunoblotting

Quantitative immunoblotting was used to assess ATP7B protein levels in WIF-B cells at various stages of Cu-responsive assays ± Baf. Briefly, WIF-B cells on coverslips were rinsed twice in PBS, scraped into 200 μl of imidazole buffer per coverslip (25 mM Imidazole, pH 7.5, 250 mM sucrose, 1 mM AEBSF, Halt protease inhibitors) and sonicated. Whole cell homogenates were diluted 6-fold using imidazole buffer to a final volume of 1200 μl, of which 5 or 6 μl was added to 2X gel sample buffer (final: 20 mM Tris·HCl, pH 8.8, 5% SDS, 0.1 M DTT, 15% sucrose, 2 mM EDTA, and 5 M urea) and heated at 50-55°C for 10min. Samples were analyzed by SDS-PAGE and Western Blotting (19). Membranes were probed with rabbit anti-ATP7B #3985-3 or mouse anti-alpha tubulin at 1:5000 or 1:6000, respectively. 3-4 experiments were done for each assay with duplicate coverslips for each condition.

Supplementary Material

Refer to Web version on PubMed Central for supplementary material.

Acknowledgments

We thank Lelita Braiterman and Arnab Gupta for critical discussions, S. Lutsenko, J. Gitlin, and A. Hasilic for antibody gifts, and Esther Kieserman (Basic Science Microscope Facility) for assistance with confocal imaging. The LSM 710 NLO microscope was obtained through a shared instrumentation grant (S10RR024550). This work was supported by NIH grants P01 DK-072084 and P01-GM067166.

References

1. Scheiber I, Dringen R, Mercer JF. Copper: effects of deficiency and overload. Metal Ions in Life Sciences. 2013; 13:359–387. [PubMed: 24470097]
2. Lutsenko S, Barnes NL, Bartee MY, Dmitriev OY. Function and regulation of human copper-transporting ATPases. Physiological Reviews. 2007; 87(3):1011–1046. [PubMed: 17615395]
3. Gupta A, Lutsenko S. Human copper transporters: mechanism, role in human diseases and therapeutic potential. Future Medicinal Chemistry. 2009; 1(6):1125–1142. [PubMed: 20454597]
4. Schaefer M, Hopkins RG, Failla ML, Gitlin JD. Hepatocyte-specific localization and copperdependent trafficking of the Wilson's disease protein in the liver. The American Journal of Physiology. 1999; 276(3 Pt 1):G639–646. [PubMed: 10070040]

5. Braiterman LT, Murthy A, Jayakanthan S, Nyasae L, Tzeng E, Gromadzka G, Woolf TB, Lutsenko S, Hubbard AL. Distinct phenotype of a Wilson disease mutation reveals a novel trafficking determinant in the copper transporter ATP7B. Proceedings of the National Academy of Sciences of the United States of America. 2014; 111(14):E1364–1373. [PubMed: 24706876]

6. Demaurex N. News in physiological sciences : an international journal of physiology produced jointly by the International Union of Physiological Sciences and the American Physiological Society. pH Homeostasis of cellular organelles. 2002; 17:1–5.

7. Beyenbach KW, Wieczorek H. The V-type H+ ATPase: molecular structure and function, physiological roles and regulation. The Journal of Experimental Biology. 2006; 209(Pt 4):577–589. [PubMed: 16449553]

8. Drose S, Altendorf K. Bafilomycins and concanamycins as inhibitors of V-ATPases and P-ATPases. The Journal of Experimental Biology. 1997; 200(Pt 1):1–8. [PubMed: 9023991]

9. Clague MJ, Urbe S, Aniento F, Gruenberg J. Vacuolar ATPase activity is required for endosomal carrier vesicle formation. The Journal of Biological Chemistry. 1994; 269(1):21–24. [PubMed: 8276796]

10. van Weert AW, Dunn KW, Geuze HJ, Maxfield FR, Stoorvogel W. Transport from late endosomes to lysosomes, but not sorting of integral membrane proteins in endosomes, depends on the vacuolar proton pump. The Journal of Cell Biology. 1995; 130(4):821–834. [PubMed: 7642700]

11. Harada M, Sakisaka S, Yoshitake M, Kin M, Ohishi M, Shakado S, Mimura Y, Noguchi K, Sata M, Tanikawa K. Bafilomycin A1, a specific inhibitor of vacuolar-type H(+)-ATPases, inhibits the receptor-mediated endocytosis of asialoglycoproteins in isolated rat hepatocytes. Journal of Hepatology. 1996; 24(5):594–603. [PubMed: 8773916]

12. Presley JF, Mayor S, McGraw TE, Dunn KW, Maxfield FR. Bafilomycin A1 treatment retards transferrin receptor recycling more than bulk membrane recycling. The Journal of Biological Chemistry. 1997; 272(21):13929–13936. [PubMed: 9153255]

13. Braiterman L, Nyasae L, Guo Y, Bustos R, Lutsenko S, Hubbard A. Apical targeting and Golgi retention signals reside within a 9-amino acid sequence in the copper-ATPase, ATP7B. American Journal of Physiology Gastrointestinal and Liver Physiology. 2009; 296(2):G433–444. [PubMed: 19033537]

14. Braiterman L, Nyasae L, Leves F, Hubbard AL. Critical roles for the COOH terminus of the Cu-ATPase ATP7B in protein stability, trans-Golgi network retention, copper sensing, and retrograde trafficking. American Journal of Physiology Gastrointestinal and Liver Physiology. 2011; 301(1):G69–81. [PubMed: 21454443]

15. Weiss KH, Lozoya JC, Tuma S, Gotthardt D, Reichert J, Ehehalt R, Stremmel W, Fullekrug J. Copper-induced translocation of the Wilson disease protein ATP7B independent of Murr1/COMMD1 and Rab7. The American Journal of Pathology. 2008; 173(6):1783–1794. [PubMed: 18974300]

16. Lalioti V, Hernandez-Tiedra S, Sandoval IV. DKWSLLL, a Versatile DXXXLL-Type Signal with Distinct Roles in the Cu -Regulated Trafficking of ATP7B. Traffic. 2014

17. Polishchuk EV, Concilli M, Iacobacci S, Chesi G, Pastore N, Piccolo P, Paladino S, Baldantoni D, van ISC, Chan J, Chang CJ, Amoresano A, Pane F, Pucci P, Tarallo A, et al. Wilson Disease Protein ATP7B Utilizes Lysosomal Exocytosis to Maintain Copper Homeostasis. Developmental Cell. 2014; 29(6):686–700. [PubMed: 24909901]

18. Harada M, Kawaguchi T, Kumemura H, Terada K, Ninomiya H, Taniguchi E, Hanada S, Baba S, Maeyama M, Koga H, Ueno T, Furuta K, Suganuma T, Sugiyama T, Sata M. The Wilson disease protein ATP7B resides in the late endosomes with Rab7 and the Niemann-Pick C1 protein. The American Journal of Pathology. 2005; 166(2):499–510. [PubMed: 15681833]

19. Guo Y, Nyasae L, Braiterman LT, Hubbard AL. NH2-terminal signals in ATP7B Cu-ATPase mediate its Cudependent anterograde traffic in polarized hepatic cells. American journal of physiology Gastrointestinal and liver physiology. 2005; 289(5):G904–916. [PubMed: 15994426]

20. McMillin GA, Travis JJ, Hunt JW. Direct measurement of free copper in serum or plasma ultrafiltrate. American Journal of Clinical Pathology. 2009; 131(2):160–165. [PubMed: 19141375]

21. Tuma PL, Nyasae LK, Backer JM, Hubbard AL. Vps34p differentially regulates endocytosis from the apical and basolateral domains in polarized hepatic cells. The Journal of Cell Biology. 2001; 154(6):1197–1208. [PubMed: 11564757]
22. Ihrke G, Martin GV, Shanks MR, Schrader M, Schroer TA, Hubbard AL. Apical plasma membrane proteins and endolyn-78 travel through a subapical compartment in polarized WIF-B hepatocytes. The Journal of Cell Biology. 1998; 141(1):115–133. [PubMed: 9531552]
23. Marshansky V, Futai M. The V-type H+-ATPase in vesicular trafficking: targeting, regulation and function. Current Opinion in Cell Biology. 2008; 20(4):415–426. [PubMed: 18511251]
24. Sobota JA, Back N, Eipper BA, Mains RE. Inhibitors of the V0 subunit of the vacuolar H+-ATPase prevent segregation of lysosomal- and secretory-pathway proteins. Journal of Cell Science. 2009; 122(Pt 19):3542–3553. [PubMed: 19737820]
25. Xie Z, Xie Y, Xu Y, Zhou H, Xu W, Dong Q. Bafilomycin A1 inhibits autophagy and induces apoptosis in MG63 osteosarcoma cells. Molecular Medicine Reports. 2014; 10(2):1103–1107. [PubMed: 24890793]
26. Li M, Khambu B, Zhang H, Kang JH, Chen X, Chen D, Vollmer L, Liu PQ, Vogt A, Yin XM. Suppression of lysosome function induces autophagy via a feedback down-regulation of MTOR complex 1 (MTORC1) activity. The Journal of Biological Chemistry. 2013; 288(50):35769–35780. [PubMed: 24174532]
27. Payne AS, Kelly EJ, Gitlin JD. Functional expression of the Wilson disease protein reveals mislocalization and impaired copper-dependent trafficking of the common H1069Q mutation. Proceedings of the National Academy of Sciences of the United States of America. 1998; 95(18): 10854–10859. [PubMed: 9724794]
28. Hanada H, Moriyama Y, Maeda M, Futai M. Kinetic studies of chromaffin granule H+-ATPase and effects of bafilomycin A1. Biochemical and Biophysical Research Communications. 1990; 170(2):873–878. [PubMed: 2143378]
29. Petris MJ, Mercer JF, Culvenor JG, Lockhart P, Gleeson PA, Camakaris J. Ligand-regulated transport of the Menkes copper P-type ATPase efflux pump from the Golgi apparatus to the plasma membrane: a novel mechanism of regulated trafficking. The EMBO ournal. 1996; 15(22): 6084–6095.
30. Lim CM, Cater MA, Mercer JF, La Fontaine S. Copperdependent interaction of dynactin subunit p62 with the N terminus of ATP7B but not ATP7A. The Journal of Biological Chemistry. 2006; 281(20):14006–14014. [PubMed: 16554302]
31. Harada M, Sakisaka S, Terada K, Kimura R, Kawaguchi T, Koga H, Kim M, Taniguchi E, Hanada S, Suganuma T, Furuta K, Sugiyama T, Sata M. A mutation of the Wilson disease protein, ATP7B, is degraded in the proteasomes and forms protein aggregates. Gastroenterology. 2001; 120(4):967–974. [PubMed: 11231950]
32. Cater MA, La Fontaine S, Shield K, Deal Y, Mercer JF. ATP7B mediates vesicular sequestration of copper: insight into biliary copper excretion. Gastroenterology. 2006; 130(2):493–506. [PubMed: 16472602]
33. Gross JB Jr, Myers BM, Kost LJ, Kuntz SM, LaRusso NF. Biliary copper excretion by hepatocyte lysosomes in the rat. Major excretory pathway in experimental copper overload. The Journal of Clinical Investigation. 1989; 83(1):30–39. [PubMed: 2910913]
34. Harada M, Sakisaka S, Yoshitake M, Shakadoh S, Gondoh K, Sata M, Tanikawa K. Biliary copper excretion in acutely and chronically copper-loaded rats. Hepatology. 1993; 17(1):111–117. [PubMed: 8423032]
35. Camacho M, Machado JD, Montesinos MS, Criado M, Borges R. Intragranular pH rapidly modulates exocytosis in adrenal chromaffin cells. Journal of Neurochemistry. 2006; 96(2):324–334. [PubMed: 16336635]
36. Bartles JR, Feracci HM, Stieger B, Hubbard AL. Biogenesis of the rat hepatocyte plasma membrane in vivo: comparison of the pathways taken by apical and basolateral proteins using subcellular fractionation. The Journal of Cell Biology. 1987; 105(3):1241–1251. [PubMed: 3654750]
37. Cullen PJ, Korswagen HC. Sorting nexins provide diversity for retromer-dependent trafficking events. Nature Cell Biology. 2012; 14(1):29–37.

38. Steinberg F, Gallon M, Winfield M, Thomas EC, Bell AJ, Heesom KJ, Tavare JM, Cullen PJ. A global analysis of SNX27-retromer assembly and cargo specificity reveals a function in glucose and metal ion transport. Nature Cell Biology. 2013; 15(5):461–471.
39. Ueno K, Saito M, Nagashima M, Kojima A, Nishinoaki S, Toshima JY, Toshima J. V-ATPase-dependent luminal acidification is required for endocytic recycling of a yeast cell wall stress sensor, Wsc1p. Biochemical and Biophysical Research Communications. 2014; 443(2):549–555. [PubMed: 24326069]
40. Kojima A, Toshima JY, Kanno C, Kawata C, Toshima J. Localization and functional requirement of yeast Na+/H+ exchanger, Nhx1p, in the endocytic and protein recycling pathway. Biochimica et Biophysica Acta. 2012; 1823(2):534–543. [PubMed: 22210050]
41. Barr VA, Hubbard AL. Newly synthesized hepatocyte plasma membrane proteins are transported in transcytotic vesicles in the bile duct-ligated rat. Gastroenterology. 1993; 105(2):554–571. [PubMed: 8335210]
42. Cassio D, Hamon-Benais C, Guerin M, Lecoq O. Hybrid cell lines constitute a potential reservoir of polarized cells: isolation and study of highly differentiated hepatoma-derived hybrid cells able to form functional bile canaliculi in vitro. The Journal of Cell Biology. 1991; 115(5):1397–1408. [PubMed: 1955480]
43. Nyasae L, Bustos R, Braiterman L, Eipper B, Hubbard A. Dynamics of endogenous ATP7A (Menkes protein) in intestinal epithelial cells: copper-dependent redistribution between two intracellular sites. American Journal of Physiology Gastrointestinal and Liver Physiology. 2007; 292(4):G1181–1194. [PubMed: 17158254]
44. Zack GW, Rogers WE, Latt SA. Automatic measurement of sister chromatid exchange frequency. The journal of Histochemistry and Cytochemistry. 1977; 25(7):741–753. [PubMed: 70454]
45. Doube M, Klosowski MM, Arganda-Carreras I, Cordelieres FP, Dougherty RP, Jackson JS, Schmid B, Hutchinson JR, Shefelbine SJ. BoneJ: Free and extensible bone image analysis in ImageJ. Bone. 2010; 47(6):1076–1079. [PubMed: 20817052]
46. Anderson RG, Falck JR, Goldstein JL, Brown MS. Visualization of acidic organelles in intact cells by electron microscopy. Proceedings of the National Academy of Sciences of the United States of America. 1984; 81(15):4838–4842. [PubMed: 6146980]

Synopsis

Cellular Cu levels regulate the localization of the Cu ATPase ATP7B. We elucidated the Cu-directed trafficking itinerary of endogenous ATP7B in polarized WIF-B cells, a cell culture model for hepatocytes. We show that the Cu-directed trafficking of ATP7B to the apical plasma membrane requires luminal acidification for sorting and exit from basolateral and subapical endosomes. Deacidifcation of luminal pH selectively blocked the Cu-directed pathway to the apical plasma membrane, while exit and return to the Golgi was largely unaffected.

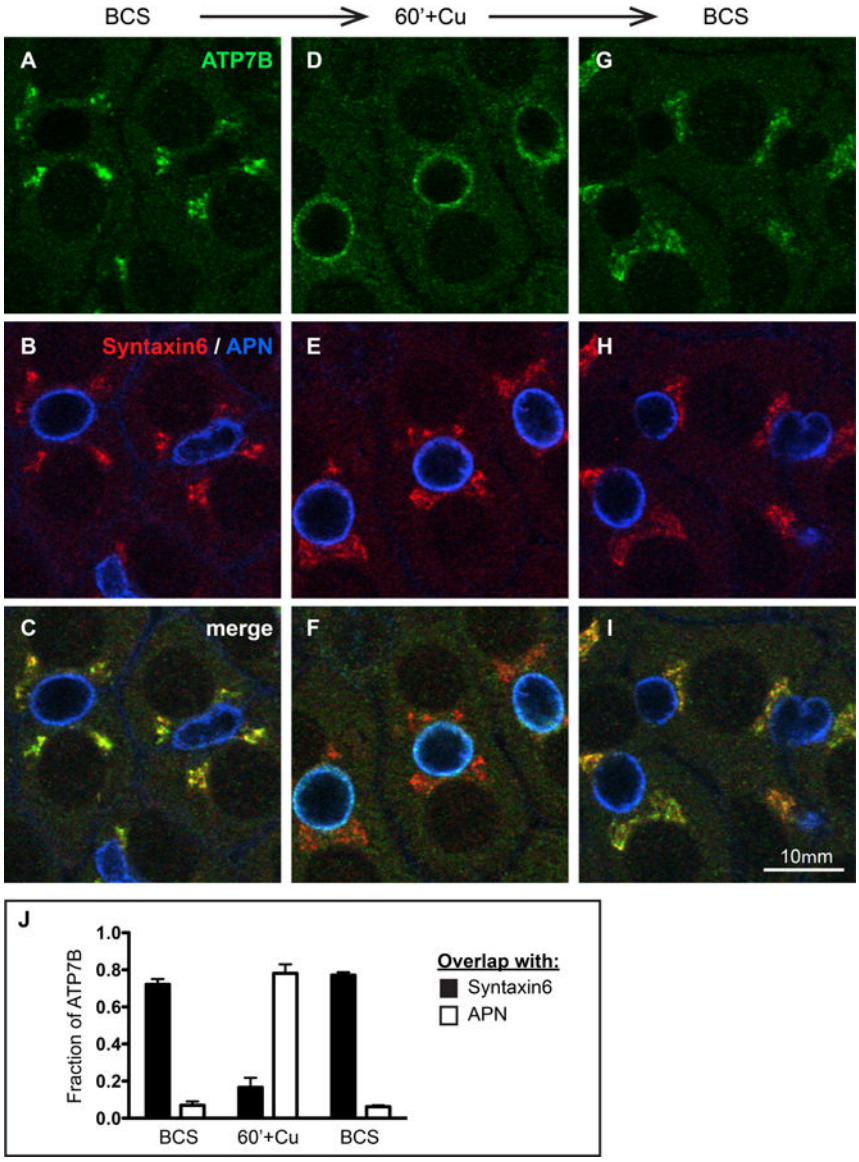

Figure 1. Cu directs the trafficking of endogenous ATP7B in WIF-B cells

A-C) WIF-B cells incubated overnight in 10 μM BCS to stage endogenous ATP7B at the TGN region. D-F) Cells switched to 10 μM $CuCl_2$ for 60 minutes. G-I) Cu-treated cells that were rinsed and re-incubated in 10 μM BCS for 180 minutes. After fixation, cells were triple-stained with antibodies to ATP7B (green), Syntaxin 6, a post-TGN marker (red) and aminopeptidase N, APN, an apical surface marker (blue). Single confocal planes are shown. J) The fraction of total ATP7B fluorescence that localized to the TGN or apical region in each condition was quantified as the extent of overlap with Syntaxin 6 or APN, respectively. Data shown represent the mean +/- SEM from at least 3 confocal stacks (approximately 28 WIF-B cells/stack, obtained from a single experiment).

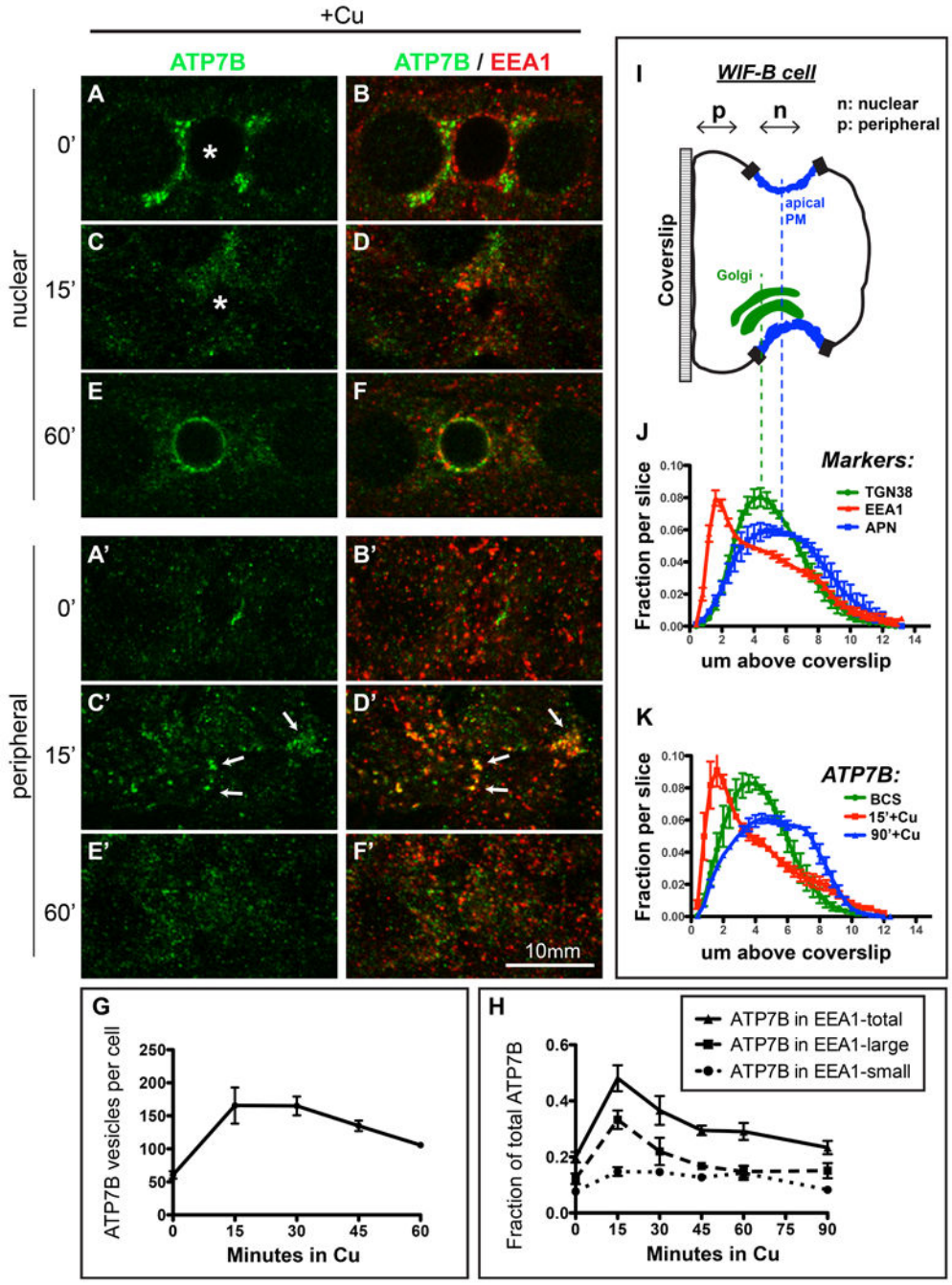

Figure 2. Cu-directed anterograde (TGN-to-apical) traffic occurs via TGN-derived vesicles that traverse an EEA1-positive compartment

A-B) WIF-B cells were incubated overnight in 10 μM BCS to stage ATP7B at the TGN region then C-D) switched to 10 μM $CuCl_2$ for 15 minutes, or E-F) 10 μM $CuCl_2$ for 60 minutes. Cells were fixed and double-stained with antibodies to ATP7B (green) and EEA1 (red) then imaged by confocal microscopy. A-F) depict single nuclear confocal planes. A'-F' depict single peripheral planes. Renderings of representative stacks from these time points are shown in the top row of Supplementary Figure S4. G) The number of ATP7B vesicles/ cell was estimated using 3D objects-based analysis. H) Fraction of ATP7B fluorescence that

was coincident with EEA1-positive small and large endosomes. Data shown in G and H represent the mean +/- SEM of at least 4 confocal stacks from a single experiment. I) Schematic cartoon of a WIF-B cell grown on a glass coverslip and rotated 90°. J) Confocal stacks were analyzed by displaying the normalized fractional distribution per slice of various organelle markers, to show the distribution of each marker along the z-plane of the cells. The Cu status of the cells had no effect on the distribution of these markers thus the data shown are pooled with no respect to Cu status, from 7-12 confocal stacks, from at least 2 independent experiments. EEA1-positive endosomes (red) distribute closer to the coverslip (∼2 μm above it) compared to the TGN38 (Golgi, green, ∼5 μm above coverslip) or APN (apical membrane, blue, ∼6 μm above coverslip). K) Cu-induced redistribution of ATP7B into a large basolateral EEA1 endosomes (15 minutes, red profile).

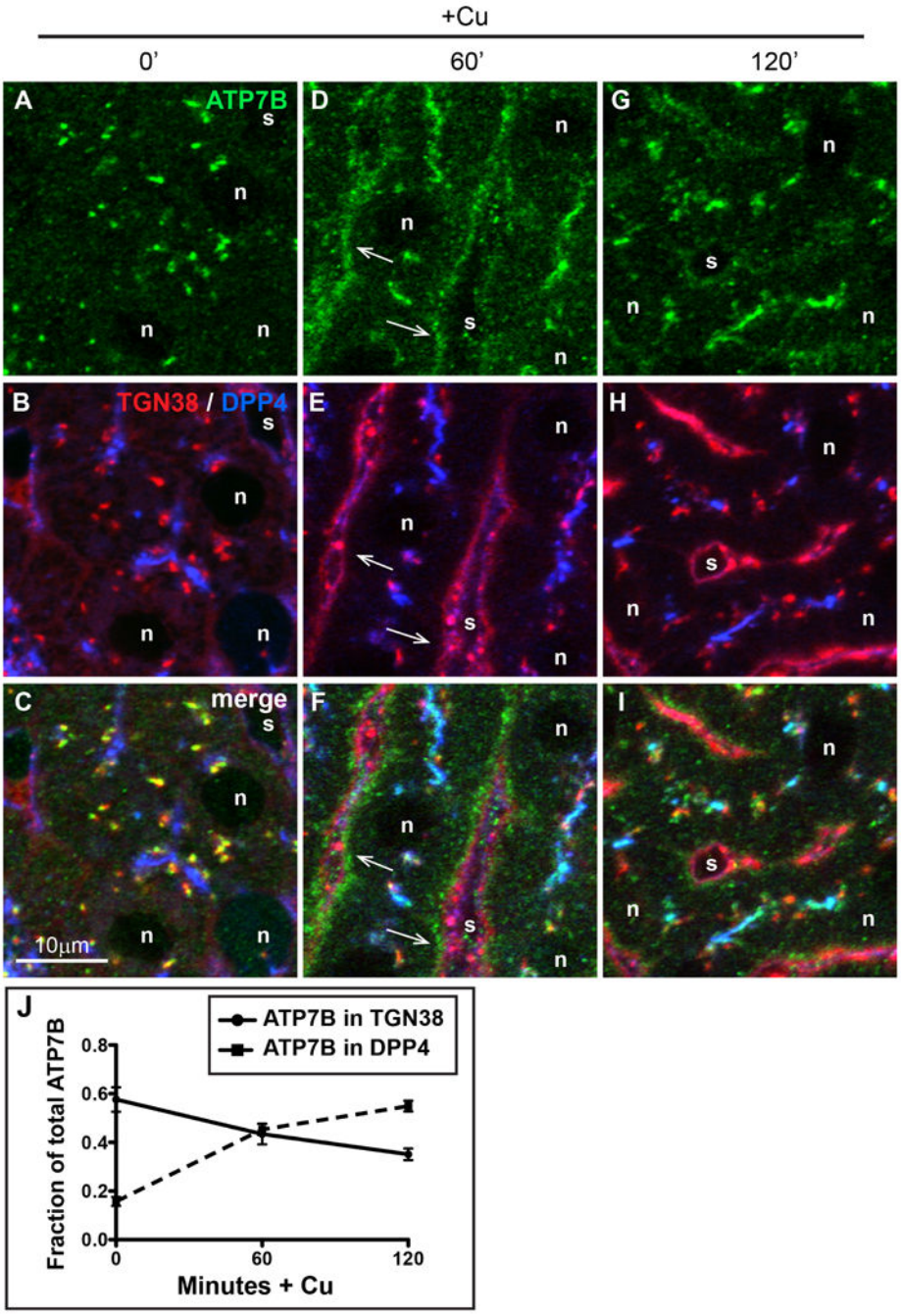

Figure 3. Cu-directed TGN-to-apical trafficking occurs via a basolateral compartment in hepatocytes in vivo

A-C) Liver section from a rat raised on a low-Cu diet for 38-45 days since birth. D-F) Liver section from a low copper rat given Cu then sacrificed after 60 minutes, or G-I) 120 minutes. Rat livers were fixed by immersion and cryosections were immunolabeled for ATP7B (green), TGN38 (red), or apical surface marker DPP4 (blue) then imaged by confocal microscopy. (G-I), Arrows indicate the transient appearance of ATP7B in the basolateral region 60 minutes after Cu injection. J) Quantification of Cu-induced trafficking in vivo. The graph depicts colocalization analysis on confocal stacks from liver sections

stained above. Cu causes a decrease of ATP7B in the Golgi (solid line), with concomitant increase in ATP7B trafficking to the apical domain (dotted line).

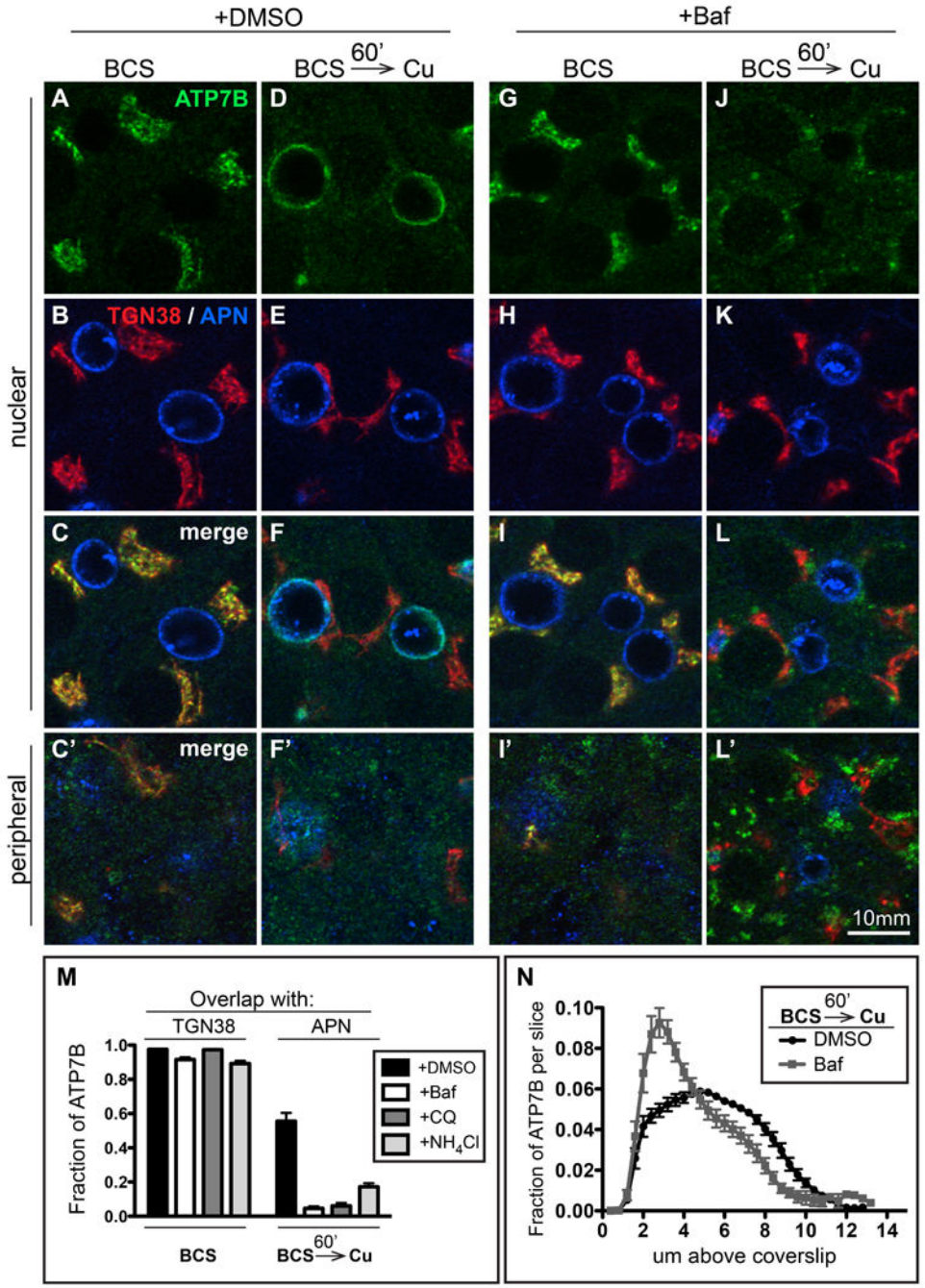

Figure 4. Treatment of WIF-B cells with Baf or weak bases prevents Cu-dependent delivery to the apical region

WIF-B cells were incubated overnight in 10 μM BCS to stage ATP7B at the TGN region. A-C) DMSO or G-I) 50 nM Baf were added for the last 30 minutes of BCS-treatment to deacidify compartments before Cu was added to induce ATP7B trafficking. Cells were then rinsed and transferred to 10 μM $CuCl_2$ for 60 minutes in the continued presence of D-F) DMSO, or J-L) 50 nM Baf. Some of the cells were fixed at each step and triple-stained with antibodies to ATP7B (green), TGN38 (red) and APN (blue) then analyzed by confocal microscopy. A-L) Single planes from the nuclear region. C', F', I' and L') Single planes from

the peripheral region. M) The overlap between ATP7B and TGN38 or APN was quantified by image analysis of the confocal stacks. Neither Baf nor the weak bases (300 μM CQ or 30 mM NH_4Cl) affected ATP7B localization at the TGN region in BCS-treated cells (left bars), but all three drugs severely impaired traffic to the apical region (right bars). N) Applying the distribution-in-z analysis used in Figure 2, we observed a distribution of ATP7B in Cu plus Baf that indicates protracted accumulation of ATP7B in a peripheral/basolateral site, presumably the structures localized at the peripheral region in the presence of Baf (compare F' and L').

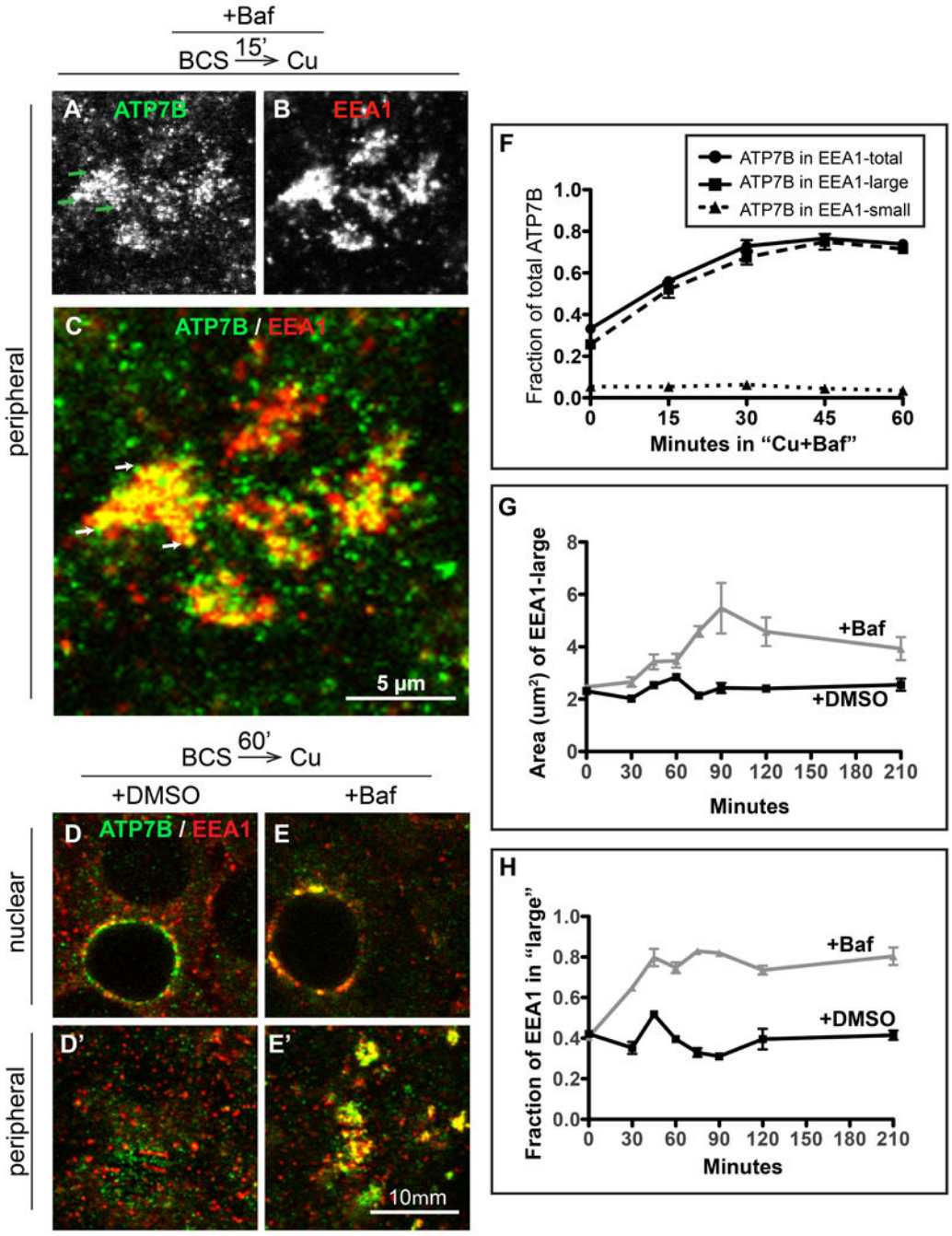

Figure 5. Baf plus Cu causes ATP7B to accumulate in large EEA1-positive endosomes located predominantly at the peripheral region of WIF-B cells

Cells were treated same as Figure 4 but fixed at 15 minute intervals during the 60 minutes of Cu-treatment plus DMSO or 50 nM Baf, then double-stained for ATP7B (green) and EEA1 (red). Substantial overlap between A) ATP7B and B) EEA1 was seen in large clusters at the peripheral region of cells as early as 15 minutes after Cu plus Baf. C) Magnification of a group of typical Baf-induced clusters (each ∼5 µm across), with ATP7B concentrated in subdomains (arrows) of the large and more homogeneous EEA1-positive endosomes. D) 60 minutes after Cu plus DMSO or E) Cu plus Baf. Single confocal planes from the D-E)

nuclear or D'-E') peripheral region show overlap between ATP7B and EEA1 persisted in Baf-treated cells. 3D renderings of confocal image stacks representing 0, 15 and 60- minute time points are shown in Supplementary Movie S4. F) The extent of overlap between ATP7B and EEA1 during 60 minutes of Cu plus Baf was quantified from at least 4 confocal stacks from a single experiment. The 0 and 60 minute time points represent the mean of 10 confocal stacks, obtained from 3 independent experiments. G) To characterize the effect of Baf on the EEA1-positive endosomes, the mean cross-sectional area of the large EEA1 structures was measured across all experimental conditions and plotted against the time that the cells were incubated in Baf or DMSO. H) The fraction of total EEA1 that was present in "large" EEA1 organelles, defined as having > 1 μm^2 cross-sectional area in the 2D analysis.

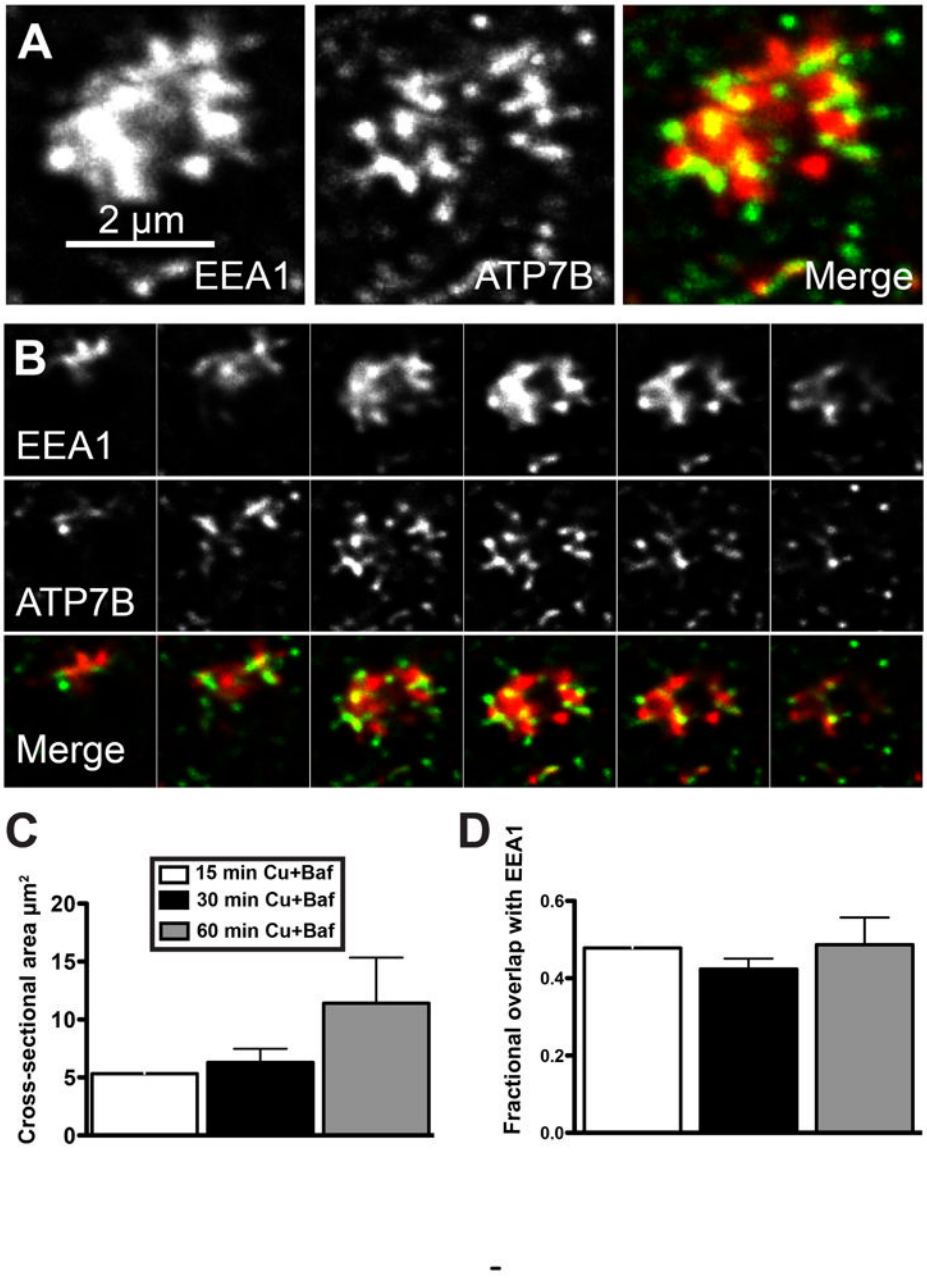

Figure 6. Detailed characterization of Baf-induced clusters of ATP7B and EEA1

WIF-B cells were treated with Cu in the presence of Baf, fixed after 15, 30, or 60 minutes, then immunolabled for EEA1 (red) and ATP7B (green). Confocal stacks were subjected to a blind deconvolution routine to enhance the signal-to-noise ratio. A) Example of a Baf-induced basolateral EEA structure from the 15 min time point (maximal Z-projection). B) Serial sections (0.25 µm steps) illustrating the close and often complementary relationship between EEA1 and ATP7B within the structure. C) Mean cross-sectional area of EEA1 channel measured at the 3 time points. D) Colocalization analysis measuring the percent of ATP7B fluorescence that was coincident with EEA1. Mean +/- S.E.M. N=22 structures analyzed.

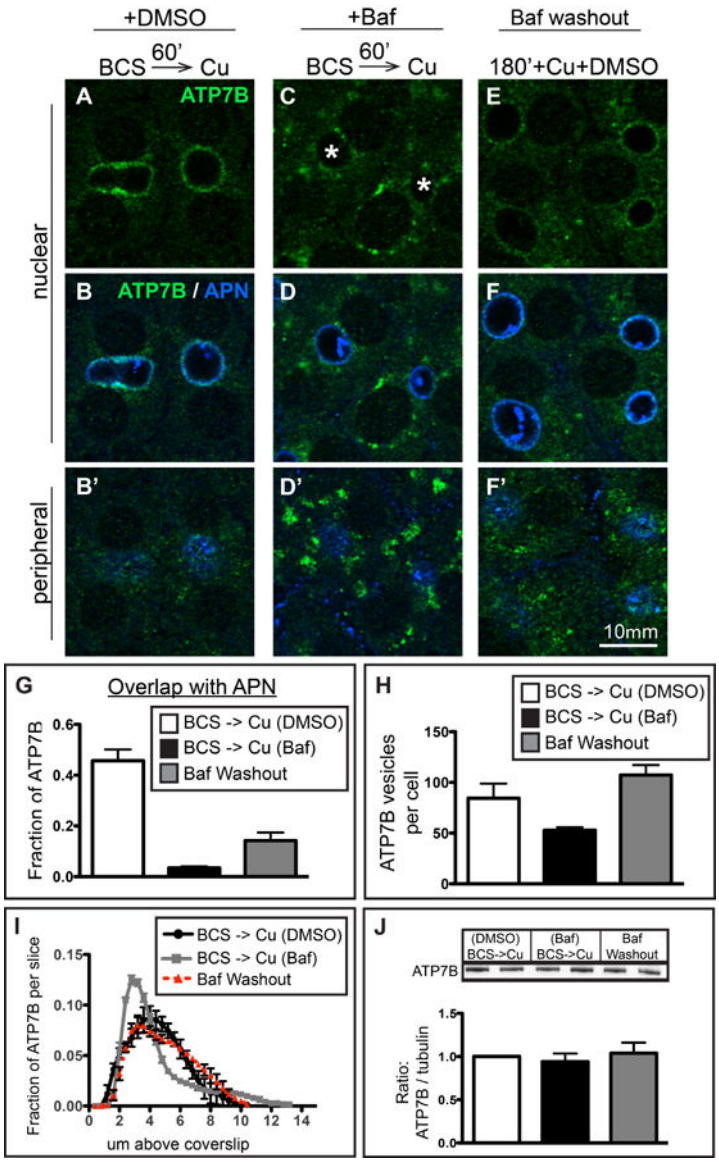

Figure 7. Removal of Baf partially restores delivery of ATP7B to the apical region in Cu-treated WIF-B cells

A-B) WIF-B cells treated 60 minutes with Cu plus DMSO or C-D) Cu plus 50 nM Baf. E-F) A parallel set of Baf-treated cells was rinsed and incubated for an additional 180 minutes in 10 μM $CuCl_2$ plus DMSO before fixation and double-stained with antibodies to ATP7B (green) and APN (blue). Cells were analyzed and imaged by confocal microscopy. A-F) Single planes from the nuclear region. B', D', F') Single planes from peripheral region. G) The extent of overlap between ATP7B and APN at the apical region indicates a partial restoration of apical targeting. H) Washout of Baf restores the number of ATP7B small vesicles to control levels. I) Axial-plane analysis of ATP7B distribution indicates a restoration of the peak ATP7B fluorescence to the typical apical region distribution. Measurements shown in graphs were performed on a minimum of 3 confocal stacks per condition, from a single experiment (approximately 84 cells). J) Western blots of ATP7B from duplicate coverslips in 4 separate experiments indicate no changes in ATP7B protein

levels due to new synthesis or aberrant lysosomal targeting due to Baf during the course of the experiment.

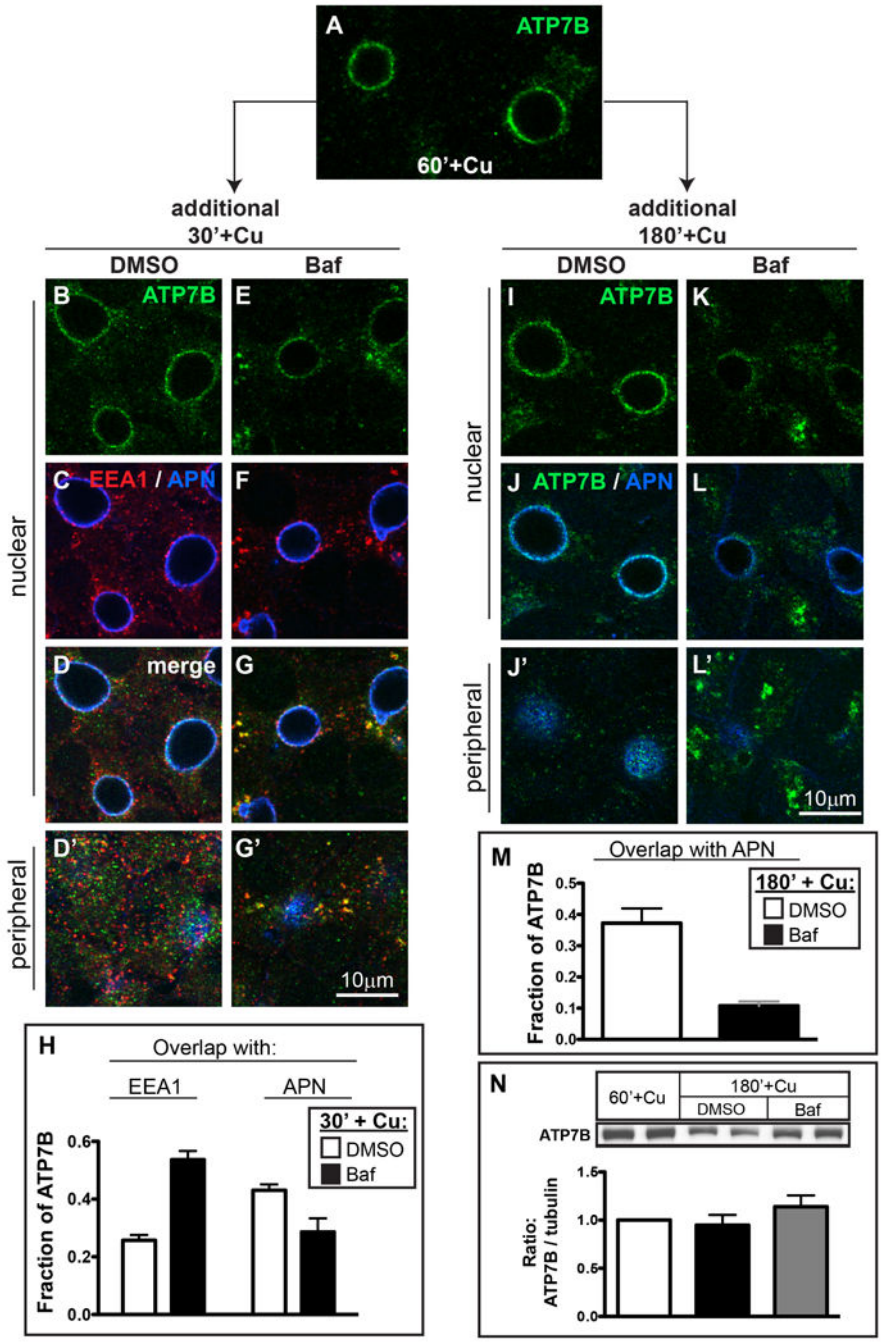

Figure 8. Cu-dependent localization of ATP7B at the apical domain is maintained by local recycling through apical endosomes and is perturbed by Baf

A) WIF-B cells were incubated overnight in 10 μM BCS then switched to 10 μM $CuCl_2$ for 60 minutes to stage ATP7B at the apical region, then fixed. B-G) Parallel sets of cells were maintained in Cu for an additional 30 minutes, or I-L) 180 minutes in the presence of B-D, I-J) DMSO, or E-G, K-L) 50 nM Baf. Cells were stained with antibodies to ATP7B (green), EEA1 (red) and APN (blue), and imaged by confocal microscopy. A-G and I-L) Single planes from the nuclear region. D', G', J' and L') Single planes from the peripheral region. H) Quantification of the extent of overlap between ATP7B and EEA1 or APN after 30 minutes

or, M) 180 minutes in Cu ± Baf. Data shown in H are the mean of 7 confocal stacks from 2 independent experiments (∼196 cells); Data in M represent 3 stacks from a single experiment (∼84 cells). N) Western blots of ATP7B from duplicate coverslips treated as in A, I and K (in 3 separate experiments) indicate no significant changes in ATP7B protein levels.

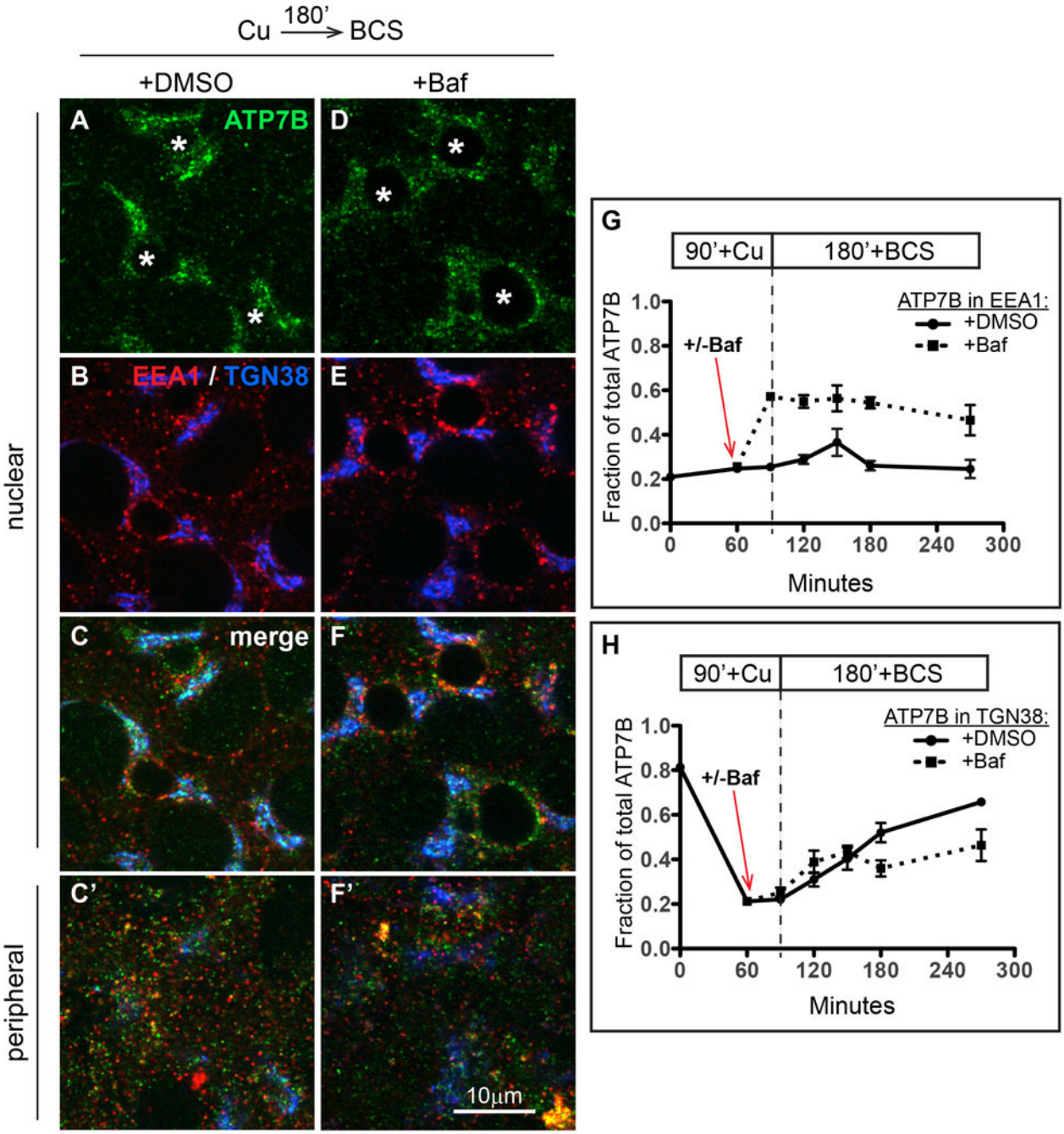

Figure 9. Cu washout initiates retrograde traffic (apical to TGN) of ATP7B, which is largely unaffected by Baf

ATP7B was staged at the apical region of WIF-B cells with Cu (see Figure 7A). Cells were then pre-incubated for 30 minutes in DMSO or Baf to deacidify intracellular compartments [see Figure 7B (+DMSO) and Figure 7E (+Baf)]. Cells were thereafter rinsed and incubated for an additional 180 minutes in 10 μM BCS to initiate retrograde traffic of ATP7B. A-C) Kinetics of ATP7B retrograde trafficking in presence of DMSO or D-F), 50 nM Baf. Cells were fixed at various times after initiating retrograde trafficking then triple-stained with antibodies to ATP7B (green), EEA1 (red) and APN (blue), analyzed and imaged by confocal

microscopy. A-F) Single planes from the nuclear region. C' and F') Single planes from the peripheral region. G) Image analysis was used to quantify the fraction of ATP7B that overlapped with EEA1, or H) TGN38. Data for each time point represent 4-7 confocal stacks from 1 or 2 independent experiments, depending on the time point.

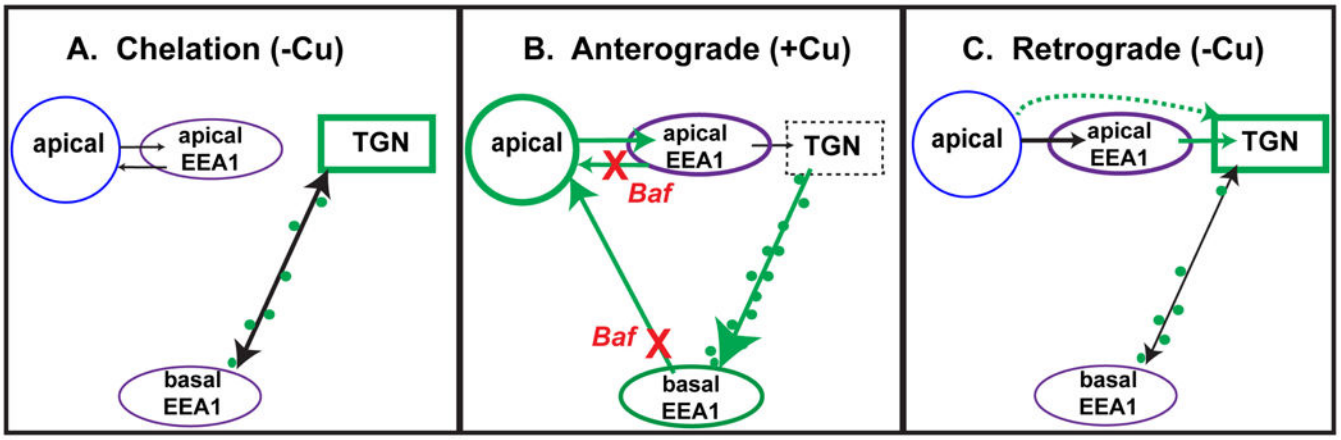

Figure 10. Summary of results

A) When Cu levels are low, about 80% of ATP7B resides in the TGN, with the remainder in small vesicles that localize near substrate side of the cell, close to the coverslip. Treatment of WIF-B cells with Baf in low Cu does not perturb localization in the TGN. B) When Cu levels are increased, this induces a rapid doubling of ATP7B vesicles, presumably derived from the TGN. These vesicles transiently traverse a pool of large EEA1-positive endosomes located near the substrate. Segregation and exit from these "basal" endosomes is inhibited by loss of luminal acidification. A second site of Baf action was revealed to be rapid recycling through an endosomal pool that lies in close association with the apical plasma membrane. Treatment with Baf promotes accumulation in these endosomes. C) When Cu is removed to induce ATP7B trafficking back to the TGN, the process proceeds similarly in the absence or presence of Baf. Thus the role of acidification is selective for ATP7B trafficking routes induced by Cu.